Biomedical Optics EXPRESS

Quantitative analysis of estimated scattering coefficient and phase retardation for ovarian tissue characterization

Yi Yang,[1,4] Tianheng Wang,[1,4] Xiaohong Wang,[2] Melinda Sanders,[2] Molly Brewer,[1,3] and Quing Zhu[1,*]

[1]*University of Connecticut, Dept. of Electrical and Computer Engineering, Storrs, CT 06269, USA*
[2]*University of Connecticut Health Center, Division of Pathology, Farmington, CT 06030, USA*
[3]*University of Connecticut Health Center, Division of Gynecologic Oncology, Farmington, CT 06030, USA*
[4]*The first two authors contributed equally to this work*
**zhu@engr.uconn.edu*

Abstract: In this report, optical scattering coefficient and phase retardation quantitatively estimated from polarization-sensitive OCT (PSOCT) were used for ovarian tissue characterization. A total of 33 *ex vivo* ovaries (normal: n = 26, malignant: n = 7) obtained from 18 patients were investigated. A specificity of 100% and a sensitivity of 86% were achieved by using estimated scattering coefficient alone; and a specificity of 100% and a sensitivity of 43% were obtained by using phase retardation alone. However, a superior specificity of 100% and sensitivity of 100% were achieved if these two parameters were used together for classifying normal and malignant ovaries. Quantitative measurement of collagen content obtained from Sirius red histology sections shows that it correlates with estimated scattering coefficient and phase retardation. Our initial results demonstrate that quantitative analysis of PSOCT could be a potentially valuable method for distinguishing normal from malignant ovarian tissues during minimally invasive surgery and help guide surgical intervention.

OCIS codes: (110.4500) Optical coherence tomography; (170.4500) Optical coherence tomography; (170.3880) Medical and biological imaging.

References and links

1. T. R. Rebbeck, H. T. Lynch, S. L. Neuhausen, S. A. Narod, L. Van't Veer, J. E. Garber, G. Evans, C. Isaacs, M. B. Daly, E. Matloff, O. I. Olopade, and B. L. Weber; Prevention and Observation of Surgical End Points Study Group, "Prophylactic oophorectomy in carriers of BRCA1 or BRCA2 mutations," N. Engl. J. Med. **346**(21), 1616–1622 (2002).
2. N. D. Kauff, J. M. Satagopan, M. E. Robson, L. Scheuer, M. Hensley, C. A. Hudis, N. A. Ellis, J. Boyd, P. I. Borgen, R. R. Barakat, L. Norton, M. Castiel, K. Nafa, and K. Offit, "Risk-reducing salpingo-oophorectomy in women with a BRCA1 or BRCA2 mutation," N. Engl. J. Med. **346**(21), 1609–1615 (2002).
3. W. A. Rocca, B. R. Grossardt, M. de Andrade, G. D. Malkasian, and L. J. Melton 3rd, "Survival patterns after oophorectomy in premenopausal women: a population-based cohort study," Lancet Oncol. **7**(10), 821–828 (2006).
4. J. S. Berek, E. Chalas, M. Edelson, D. H. Moore, W. M. Burke, W. A. Cliby, and A. Berchuck; Society of Gynecologic Oncologists Clinical Practice Committee, "Prophylactic and risk-reducing bilateral salpingo-oophorectomy: recommendations based on risk of ovarian cancer," Obstet. Gynecol. **116**(3), 733–743 (2010).
5. D. Huang, E. A. Swanson, C. P. Lin, J. S. Schuman, W. G. Stinson, W. Chang, M. R. Hee, T. Flotte, K. Gregory, C. A. Puliafito, and J. G. Fujimoto, "Optical coherence tomography," Science **254**(5035), 1178–1181 (1991).
6. E. M. Kanter, R. M. Walker, S. L. Marion, M. Brewer, P. B. Hoyer, and J. K. Barton, "Dual modality imaging of a novel rat model of ovarian carcinogenesis," J. Biomed. Opt. **11**(4), 041123 (2006).
7. L. P. Hariri, G. T. Bonnema, K. Schmidt, A. M. Winkler, V. Korde, K. D. Hatch, J. R. Davis, M. A. Brewer, and J. K. Barton, "Laparoscopic optical coherence tomography imaging of human ovarian cancer," Gynecol. Oncol. **114**(2), 188–194 (2009).
8. C. L. Evans, I. Rizvi, T. Hasan, and J. F. de Boer, "*In vitro* ovarian tumor growth and treatment response dynamics visualized with time-lapse OCT imaging," Opt. Express **17**(11), 8892–8906 (2009).
9. Y. Yang, X. Li, T. Wang, P. D. Kumavor, A. Aguirre, K. K. Shung, Q. Zhou, M. Sanders, M. Brewer, and Q. Zhu, "Integrated optical coherence tomography, ultrasound and photoacoustic imaging for ovarian tissue characterization," Biomed. Opt. Express **2**(9), 2551–2561 (2011).

#164882 - $15.00 USD Received 21 Mar 2012; revised 14 May 2012; accepted 18 May 2012; published 7 Jun 2012

10. M. A. Brewer, U. Utzinger, J. K. Barton, J. B. Hoying, N. D. Kirkpatrick, W. R. Brands, J. R. Davis, K. Hunt, S. J. Stevens, and A. F. Gmitro, "Imaging of the ovary," Technol. Cancer Res. Treat. **3**(6), 617–627 (2004).
11. Y. Yang, N. C. Biswal, T. Wang, P. D. Kumavor, M. Karimeddini, J. Vento, M. Sanders, M. Brewer, and Q. Zhu, "Potential role of a hybrid intraoperative probe based on OCT and positron detection for ovarian cancer detection and characterization," Biomed. Opt. Express **2**(7), 1918–1930 (2011).
12. Y. Yang, T. Wang, N. C. Biswal, X. Wang, M. Sanders, M. Brewer, and Q. Zhu, "Optical scattering coefficient estimated by optical coherence tomography correlates with collagen content in ovarian tissue," J. Biomed. Opt. **16**(9), 090504 (2011).
13. M. R. Hee, D. Huang, E. A. Swanson, and J. G. Fujimoto, "Polarization-sensitive low-coherence reflectometer for birefringence characterization and ranging," J. Opt. Soc. Am. B **9**(6), 903–908 (1992).
14. J. F. de Boer, T. E. Milner, M. J. C. van Gemert, and J. S. Nelson, "Two-dimensional birefringence imaging in biological tissue by polarization-sensitive optical coherence tomography," Opt. Lett. **22**(12), 934–936 (1997).
15. B. Cense, T. C. Chen, B. H. Park, M. C. Pierce, and J. F. de Boer, "Thickness and birefringence of healthy retinal nerve fiber layer tissue measured with polarization-sensitive optical coherence tomography," Invest. Ophthalmol. Vis. Sci. **45**(8), 2606–2612 (2004).
16. B. Elmaanaoui, B. Wang, J. C. Dwelle, A. B. McElroy, S. S. Liu, H. G. Rylander, and T. E. Milner, "Birefringence measurement of the retinal nerve fiber layer by swept source polarization sensitive optical coherence tomography," Opt. Express **19**(11), 10252–10268 (2011).
17. M. C. Pierce, R. L. Sheridan, B. Hyle Park, B. Cense, and J. F. de Boer, "Collagen denaturation can be quantified in burned human skin using polarization-sensitive optical coherence tomography," Burns **30**(6), 511–517 (2004).
18. J. Strasswimmer, M. C. Pierce, B. H. Park, V. Neel, and J. F. de Boer, "Polarization-sensitive optical coherence tomography of invasive basal cell carcinoma," J. Biomed. Opt. **9**(2), 292–298 (2004).
19. S. Sakai, M. Yamanari, A. Miyazawa, M. Matsumoto, N. Nakagawa, T. Sugawara, K. Kawabata, T. Yatagai, and Y. Yasuno, "*In vivo* three-dimensional birefringence analysis shows collagen differences between young and old photo-aged human skin," J. Invest. Dermatol. **128**(7), 1641–1647 (2008).
20. S. K. Nadkarni, M. C. Pierce, B. H. Park, J. F. de Boer, P. Whittaker, B. E. Bouma, J. E. Bressner, E. Halpern, S. L. Houser, and G. J. Tearney, "Measurement of collagen and smooth muscle cell content in atherosclerotic plaques using polarization-sensitive optical coherence tomography," J. Am. Coll. Cardiol. **49**(13), 1474–1481 (2007).
21. W. C. Kuo, N. K. Chou, C. Chou, C. M. Lai, H. J. Huang, S. S. Wang, and J. J. Shyu, "Polarization-sensitive optical coherence tomography for imaging human atherosclerosis," Appl. Opt. **46**(13), 2520–2527 (2007).
22. D. Fried, J. Xie, S. Shafi, J. D. B. Featherstone, T. M. Breunig, and C. Le, "Imaging caries lesions and lesion progression with polarization sensitive optical coherence tomography," J. Biomed. Opt. **7**(4), 618–627 (2002).
23. Y. Chen, L. Otis, D. Piao, and Q. Zhu, "Characterization of dentin, enamel, and carious lesions by a polarization-sensitive optical coherence tomography system," Appl. Opt. **44**(11), 2041–2048 (2005).

1. Introduction

Ovarian cancer has the lowest survival rates of the gynecologic cancers because it is predominantly diagnosed in late stages due to the lack of distinctive early symptoms as well as the lack of efficacious screening and diagnostic techniques. Currently, prophylactic oophorectomy (PO) has been accepted as the standard of care for high risk women [1,2]. PO reduces the risk of ovarian cancer by more than 50%. However, there appears to be a higher mortality for premenopausal oophorectomy and these high risk women are not candidates for hormone replacement therapy because of their increased risk of breast cancer [3]. It has recently been found that PO increases the mortality of women undergoing oophorectomy prior to the age of 45 [3] or even before the age of 55 to 60 [4]. As a result, there is an urgent need to develop more sensitive tools to effectively evaluate the ovary and identify early ovarian cancers from benign changes during minimally invasive surgery so that the use of PO can be minimized and the patients' quality of life can be improved.

Optical coherence tomography (OCT) is an emerging high resolution imaging technique [5], which measures backscattered light generated from an infrared light source directed to the tissues being examined. The morphological features of pre-neoplastic or early neoplastic changes have prompted the development of OCT for early-stage ovarian cancer detection [6–12]. OCT is sensitive to the changes in collagen which are typically seen as malignancy develops [10–12]. Polarization-sensitive OCT (PSOCT) is a functional extension of conventional OCT and offers additional physiological information by measuring the polarization properties of biological tissues [13,14]. PSOCT provides enhanced image contrast by making use of relative phase change of two orthogonal polarization detection channels. PSOCT has been reported as an effective tool to detect and analyze fibrous tissues, including retinal nerve fiber layer [15,16], collagen fibers in skin [17–19], collagen and smooth muscle cell content in atherosclerotic plaques [20,21], and carious lesions [22,23]. M.

#164882 - $15.00 USD Received 21 Mar 2012; revised 14 May 2012; accepted 18 May 2012; published 7 Jun 2012

C. Pierce *et al.* [17] quantified the birefringence loss due to thermal denaturation of collagen, with mean phase retardation rate of 0.249 degree/μm measured from 26 burned skin sites, compared with that of 0.401 degree/μm from 26 normal skin sites. J. Strasswimmer *et al*. [18] indicated that PSOCT can distinguish normal skin from tumor, and the tumor showed very little birefringence property, with the phase retardation rate much smaller than that of normal skin. S. K. Nadkarni *et al.* [20] demonstrated that PSOCT was capable of measuring the birefringence in plaques and in fibrous caps of necrotic core fibroatheroma after examining 87 aortic plaques obtained from 20 human cadavers. W. Kuo *et al.* [21] demonstrated that PSOCT enabled differentiation of the atherosclerotic structures from normal tissue, and the quantified phase retardation results indicated that birefringence changes in fibrous and calcified plaques were more apparent than in normal vessels.

In this paper, we report, to the best of our knowledge, the first study that uses PSOCT for ovarian tissue characterization. A total of 33 *ex vivo* ovaries obtained from 18 patients were evaluated. We also measured the optical scattering properties of these ovaries from conventional OCT images and evaluated the potential of using two parameters of phase retardation and scattering property to quantitatively characterize normal and malignant ovarian tissues. In our initial study, optical scattering properties were found to be a valuable parameter in distinguishing normal from malignant ovarian tissues [12]. The optical scattering coefficient and phase retardation from normal and malignant ovaries were extracted from conventional OCT and phase retardation images, respectively. The correlation between collagen content, as assessed from Sirius Red staining, estimated scattering coefficient and phase retardation properties were also investigated. Results demonstrate that scattering coefficient and phase retardation obtained from PSOCT are potentially valuable parameters in differentiating normal from malignant ovaries.

2. Materials and methods

2.1. PSOCT

Figure 1 depicts the time-domain PSOCT system configuration. The technical details of the system were described in our previous publication [23]. The key system features are briefly summarized here. The PSOCT system consists of a 40 nm bandwidth super luminescent diode

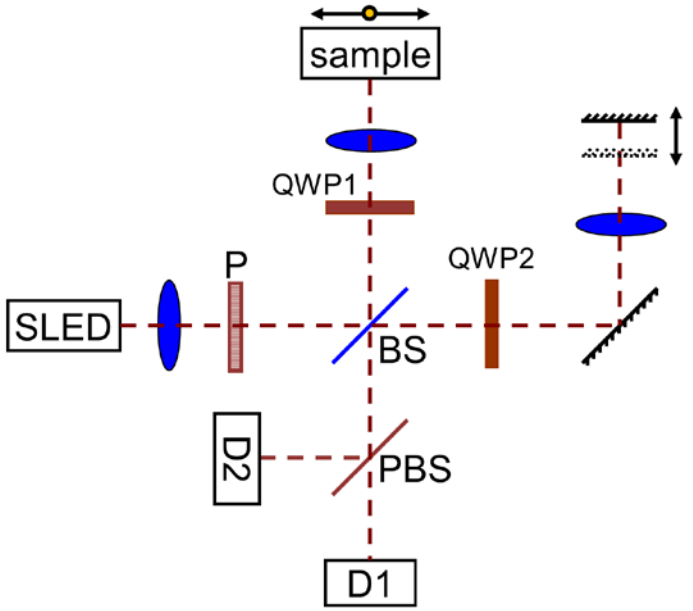

Fig. 1. Time domain polarization-sensitive OCT system configuration. P: polarizer; BS: beam splitter; PBS: polarization beam splitter.

#164882 - $15.00 USD Received 21 Mar 2012; revised 14 May 2012; accepted 18 May 2012; published 7 Jun 2012

source (SLED) at center wavelength of 1310 nm and a Michelson interferometer. The 2 mW output light beam from the SLED passes a vertical polarizer and is evenly separated into sample arm and reference arm by a beam splitter (BS). In the sample arm, a quarter-wave plate QWP1 with the fast axis oriented at 45 degrees with respect to the horizontal direction is used to convert the linearly polarized light into the circularly polarized light. The circularly polarized light is focused by an objective lens to illuminate the examined sample. In the reference arm, another quarter-wave plate QWP2 with the fast axis oriented at 22.5 degrees with respect to the horizontal direction is placed right after the BS. After light beam back-propagating through the QWP2, the polarization state is changed to 45 degrees with respect to the horizontal direction which provides equal reference power for both orthogonal polarization channels. The reference mirror is driven by a stepper motor back and forth to provide 3.6 mm free space scanning depth. The back-scattered sample arm beam and the back-reflected reference arm beam recombine and form interferogram at the BS. The recombined light is separated by a polarization beam splitter (PBS) into horizontal and vertical components which are independently directed toward two identical photodetectors (D1 and D2). Conventional OCT is obtained by calculating the summation of the squares of both orthogonal polarization channel signals. Phase retardation image is obtained from measuring the arctangent between vertical and horizontal components.

2.2. Optical scattering coefficient and phase retardation

During imaging, similar conditions for all ovarian samples were achieved by mounting the ovary on a three-dimensional stage and adjusting tissue surface to the same depth position. The calculated numerical aperture 0.02 of the sample arm optics in our fixed focusing PSOCT system was very low, which ensured the superficial scanning depth within the focal zone. Optical scattering coefficient was estimated by fitting compounded conventional OCT signal to a single scattering model based on Beer's law [12]. In this study, 1 mm tissue corresponding to 74 A-lines was selected for averaging to minimize the speckle noise effect. A fitting example from a normal ovary is shown in Fig. 2 where 2(a) is a conventional OCT image and 2(b) shows the fitting curves. The white dashed rectangular in Fig. 2(a) represents the selected 1mm area for fitting. The depth profile of one single A-line in the selected area is

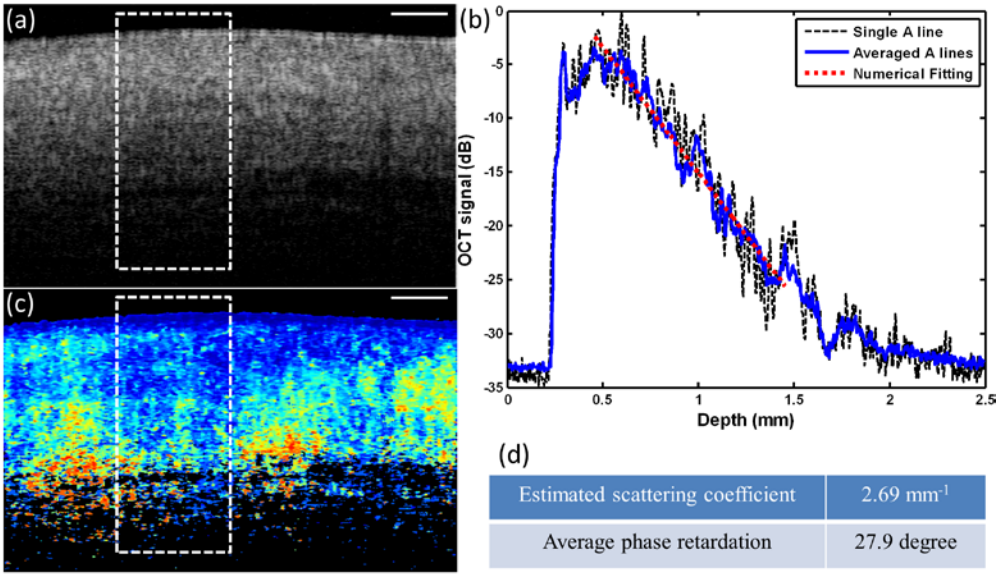

(d)

Estimated scattering coefficient	2.69 mm^{-1}
Average phase retardation	27.9 degree

Fig. 2. Optical scattering coefficient and average phase retardation measurement example. (a) conventional OCT image; (b) fitting curves; (c) phase retardation image; (d) result table. White dashed rectangular: selected area for fitting; scale bar: 0.5 mm.

#164882 - $15.00 USD Received 21 Mar 2012; revised 14 May 2012; accepted 18 May 2012; published 7 Jun 2012

plotted as the black dashed curve and the compounded depth profile is shown as the blue solid curve in Fig. 2(b). The scattering coefficient was estimated by numerically fitting the compounded depth profile to the single scattering model shown as the red dotted curve in Fig. 2(b) and the value of 2.69 mm^{-1} is shown in Fig. 2(d). The phase retardation image is shown in Fig. 2(c). The dark blue represents phase retardation value of zero degree and the dark red shows phase retardation at 90 degrees. The average phase retardation of the same area marked by the selected white dashed rectangular in Fig. 2(c) was calculated and the value of 27.9 degrees is shown in Fig. 2(d) as well.

To calculate the specificity and sensitivity, thresholds of estimated scattering coefficient and phase retardation were selected, respectively. The specificity and sensitivity of each method were calculated as: specificity = TN/(TN + FP) × 100%; sensitivity = TP/(TP + FN) × 100%, where TP represents the number of true-positive findings, TN represents the number of true negative findings, FP represents the number of false-positive findings, and FN represents the number of false-negative findings.

2.3. Ovary sample

In this study, 33 ovaries obtained from 18 patients whose age ranged from 37 to 78 (mean 61) were investigated using the PSOCT system. Ovaries were extracted from patients undergoing PO at the University of Connecticut Health Center (UCHC). The patients were at risk for ovarian cancer or they had an ovarian mass suggestive of malignancy. This study was approved by the Institutional Review Boards of UCHC, and informed consent was obtained from all patients. Ovaries were kept in the 0.9% wt/vol NaCl solution and imaged within 24 hours after oophorectomy. After PSOCT imaging, the ovaries were fixed in 10% formalin solution and returned to the Pathology Department for histological processing.

2.4. Histopathology and collagen area fraction

For histological evaluation, the ovaries were cut in 5 mm blocks parallel to the imaging plane, dehydrated with graded alcohol, embedded in paraffin and sectioned to 7 μm thickness using a paraffin microtome. Once the slides that correspond to the imaged planes were identified, they were stained using hematoxylin and eosin (H&E) for diagnosis. In addition, in order to analyze the collagen content, adjacent cross-section (7 μm apart from H&E cross-section) was sliced and Sirius Red staining protocol which specifically binds to collagen was applied to these slides. The digital image of histological ovarian surface tissue covering about 1 mm depth was acquired using a bright field microscope. The collagen content was quantitatively calculated using ImageJ software (National Institutes of Health). The collagen area fraction (CAF) was measured as "Stained collagen area/tissue area."

3. Results and discussion

Figure 3 shows one comparison example between normal [Figs. 3(a)–3(b)] and malignant [Figs. 3(c)–3(d)] ovarian tissue. Figure 3(a) and 3(c) are conventional OCT images, while 3(b) and 3(d) are phase retardation images. The mean values of estimated scattering coefficients for Figs. 3(a) and 3(c) are 3.07 mm^{-1} and 0.85 mm^{-1}, respectively. The mean values of phase retardation for Figs. 3(b) and 3(d) are 30.0 and 12.9 degrees, respectively.

A total of 18 patients and 33 ovaries were imaged using the PSOCT system. Three patients (#13, #14 and #17) each had only one ovary available for this study. Twenty six ovaries obtained from 15 patients were diagnosed as normal and 7 ovaries obtained from 4 patients were diagnosed as malignant. One patient (#10) had her left ovary diagnosed as malignant and her right ovary diagnosed as normal. The patient category, age, mean estimated scattering coefficient, mean phase retardation and mean CAF value are summarized in Table 1.

Depending on the size of the examined ovary, 34~142 measurements of scattering coefficient and phase retardation were performed for each ovary. A total of 2044 scattering coefficients and phase retardation values were estimated from these 33 ovaries while 1427 from 26 normal ones and 617 from 7 malignant ones. A total of 1072 CAFs were measured from Sirius Red staining histology while 859 from the normal group and 213 from the

#164882 - $15.00 USD Received 21 Mar 2012; revised 14 May 2012; accepted 18 May 2012; published 7 Jun 2012

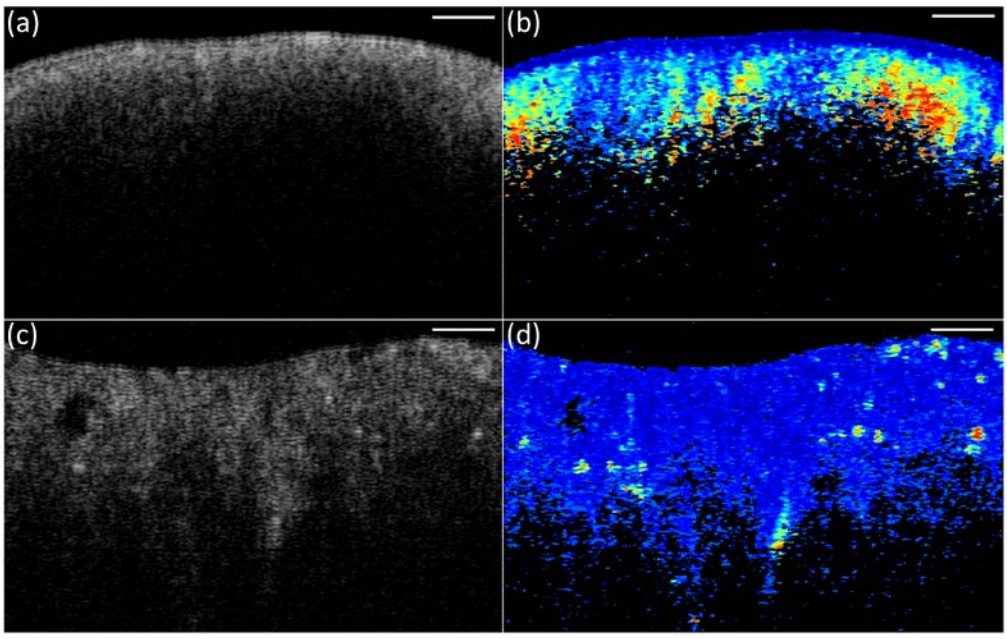

Fig. 3. Conventional OCT (a, c) and phase retardation images (b, d) from normal (a, b) and malignant (c, d) ovarian tissue. Scale bar: 0.5 mm.

malignant group. The histograms of estimated scattering coefficient, phase retardation and CAF for normal and malignant groups are shown in Figs. 4(a)–4(c), respectively. The blue bar represents the normal group and the red bar represents the malignant group. Estimated scattering coefficient in normal and malignant ovarian tissue shows Gaussian distribution property demonstrated as the dotted and solid curves in Fig. 4(a). The normal group has higher scattering property at a wavelength of 1310 nm ranging from 0.60 to 5.27 mm^{-1} with a mean value of 2.38 mm^{-1} (±0.67), while the malignant group demonstrates lower value ranging from 0.42 to 3.86 mm^{-1} with a mean value of 1.74 mm^{-1} (±0.55). For phase retardation shown in Fig. 4(b), the normal group has higher values ranging from 8.7 to 60.6 degrees with a mean value of 22.6 degrees (±9.0 degrees) while the malignant group demonstrates lower value ranging from 9.9 to 53.8 degrees with a mean value of 19.1 degrees (±9.4 degrees). For CAF shown in Fig. 4(c), the normal group has higher collagen content ranging from 7.6% to 81.0% with a mean value of 47.8% (±15.4%) and the malignant group has lower value ranging from 4.6% to 61.7% with a mean value of 26.2% (±11.6%). CAF in normal and malignant ovarian tissue shows Gaussian distribution property as demonstrated by dotted and solid curves in Fig. 4(c).

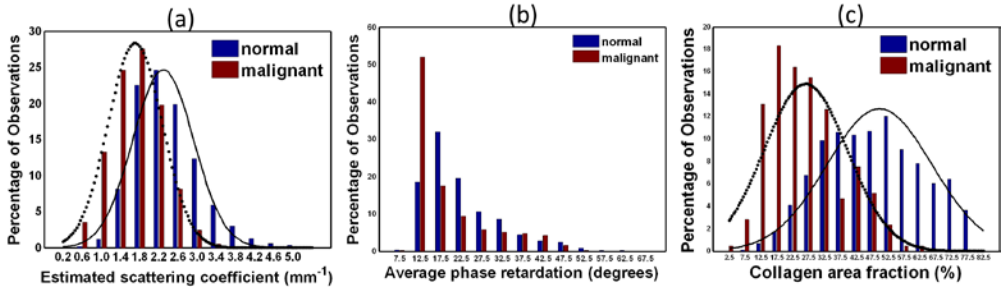

Fig. 4. Histograms of estimated scattering coefficient (a), phase retardation (b) and collagen area fraction (c) for normal and malignant ovary groups.

#164882 - $15.00 USD Received 21 Mar 2012; revised 14 May 2012; accepted 18 May 2012; published 7 Jun 2012

Table 1. Patient information and measurement results

Category	Patient No.	Age (years)	Left (L) Right (R)	Estimated scattering coefficient (mm^{-1})	Phase retardation (degrees)	Collagen area fraction (%)
Normal	1	65	L	2.31	22.2	36.3
			R	2.12	36.6	43.8
	2	73	L	2.38	31.0	53.6
			R	2.14	24.6	45.3
	4	42	L	2.25	22.5	40.7
			R	2.29	16.4	53.7
	5	55	L	2.36	24.7	58.4
			R	2.26	18.2	47.7
	6	74	L	2.53	20.6	54.1
			R	2.29	21.2	37.1
	7	58	L	3.00	21.7	44.2
			R	2.24	17.7	46.2
	8	79	L	2.15	16.1	25.1
			R	2.28	23.1	46.9
	9	79	L	2.50	25.9	42.6
			R	2.75	22.5	38.0
	10	53	R	2.27	28.5	56.8
	11	48	L	2.34	16.8	43.9
			R	2.35	28.2	44.6
	12	47	L	2.47	21.3	44.6
			R	2.52	24.2	56.4
	13	45	L	2.39	17.8	42.9
	14	37	L	2.23	32.1	63.4
	16	72	L	2.77	21.3	60.0
			R	2.60	17.1	39.5
	17	48	L	2.23	15.8	30.5
	mean ± standard deviation			2.39 ± 0.21	22.6 ± 5.3	46.0 ± 9.1
Malignant	3	77	L	1.77	31.4	32.9
			R	1.60	17.9	18.8
	10	53	L	1.90	25.9	42.8
	15	71	L	1.98	25.7	32.6
			R	1.10	14.7	23.3
	18	76	L	2.16	14.7	22.0
			R	1.81	11.9	26.7
	mean ± standard deviation			1.76 ± 0.34	20.3 ± 7.4	28.4 ± 8.3

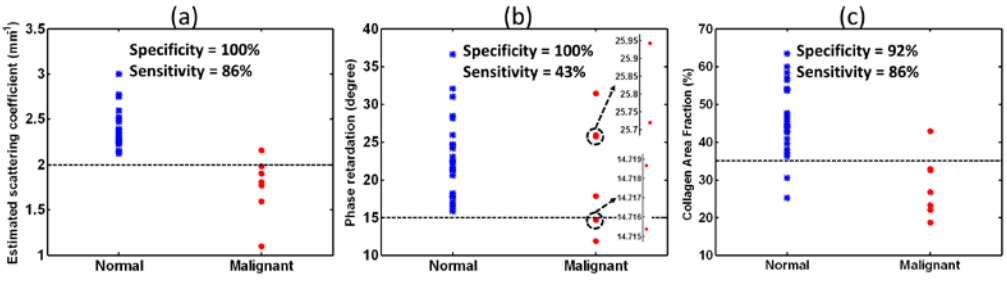

Fig. 5. Scatter plots of estimated scattering coefficient (a), phase retardation (b) and CAF (c) of each ovary for normal and malignant ovary groups.

The scatter plots in Figs. 5(a)–5(c) show mean estimated scattering coefficient, mean phase retardation and mean CAF value of each ovary for normal and malignant groups, respectively. Using estimated scattering coefficient as a classifier and selecting the separation threshold at 2 mm^{-1}, a specificity of 100% and a sensitivity of 86% are achieved. Especially for patient #10 who had left ovary diagnosed as malignant and right ovary diagnosed as normal, her bilateral ovaries are classified into correct groups based on estimated scattering coefficient. The mean value of estimated scattering coefficient of each ovary for normal and malignant groups, along with their standard deviation, is listed in Table 1. The Student's t-test shows statistical significance between normal and malignant groups with a p value of 0.002.

#164882 - $15.00 USD Received 21 Mar 2012; revised 14 May 2012; accepted 18 May 2012; published 7 Jun 2012

Using phase retardation as a classifier and selecting the separation threshold at 15 degrees, a specificity of 100% and a sensitivity of 43% are achieved. For the two insets pointed by the dashed circle-arrows shown in Fig. 5(b), each shows two ovaries with close values. The mean value and standard deviation of phase retardation of each ovary for normal and malignant groups are also listed in Table 1 and are not statistically significant ($p = 0.462$) between normal and malignant groups. However, the phase retardation images show very different features as shown in Figs. 3(b) and 3(d) which could help characterize ovarian tissue qualitatively. In Fig. 3(b) the phase retardation of the normal ovarian tissue increases uniformly and is slightly dependent on the depth. But in Fig. 3(d) the phase retardation of the malignant ovarian tissue shows more random manner with red spots scattered in the image sporadically. Although using CAF alone as a classifier it can't completely differentiate normal from malignant ovaries (specificity 92% and sensitivity 86%) as shown in Fig. 5(c), statistical significance between normal (46.0% ± 9.1%, n = 26) and malignant (28.4% ± 8.3%, n = 7) groups was found with a p value less than 0.0001.

Combining estimated scattering coefficient and phase retardation for each ovary, we should be able to differentiate normal and malignant ovaries more effectively. The scatter plot in Fig. 6 shows the two parameters for each ovary. The blue star represents normal ovary and the red circle represents malignant ovary. The centers and half axes of blue and red solid ellipses show the mean value and standard deviation of estimated scattering coefficient and phase retardation for each group. Using estimated scattering coefficient and phase retardation as the classifiers and selecting the same thresholds at 2 mm^{-1} and 15 degrees shown as the green dashed lines in Fig. 6, 100% specificity and 100% sensitivity can be obtained.

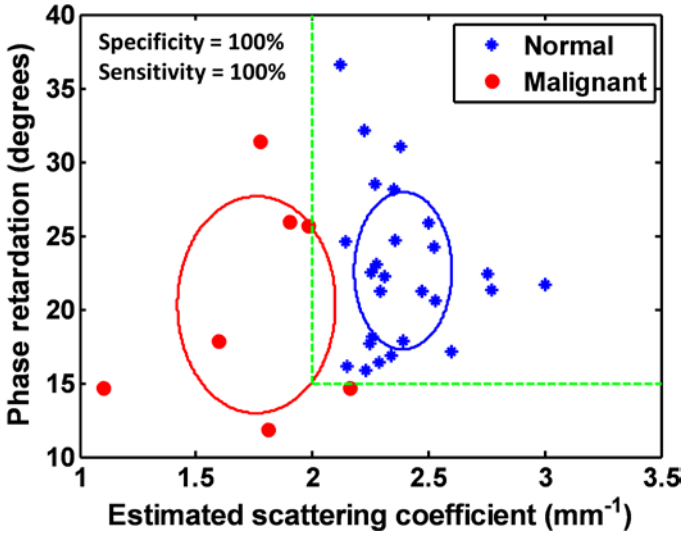

Fig. 6. Two-parameter (estimated scattering coefficient and average phase retardation) plot.

Linear regression analysis in Fig. 7(a) shows positive correlation between collagen content and estimated scattering coefficient with R value of 0.57 ($p < 0.0001$). Phase retardation measured from ovaries is also positively correlated with collagen content with R value of 0.47 ($p < 0.01$) which is shown in Fig. 7(b). The blue dashed plots show the 95% prediction intervals. The different collagen content found in normal and malignant groups in part explains the different scattering properties estimated from conventional OCT measurements and the different birefringence behaviors from phase retardation images. However, there are many other factors, including collagen thickness, collagen orientation, fibroblast and cell nuclei, etc., which may need to take into account. In addition, note that in this CAF study, there are 1072 measurements which are less than the 2044 scattering coefficient and phase retardation measurements and these CAF measurements are obtained from close sites but not

#164882 - $15.00 USD Received 21 Mar 2012; revised 14 May 2012; accepted 18 May 2012; published 7 Jun 2012

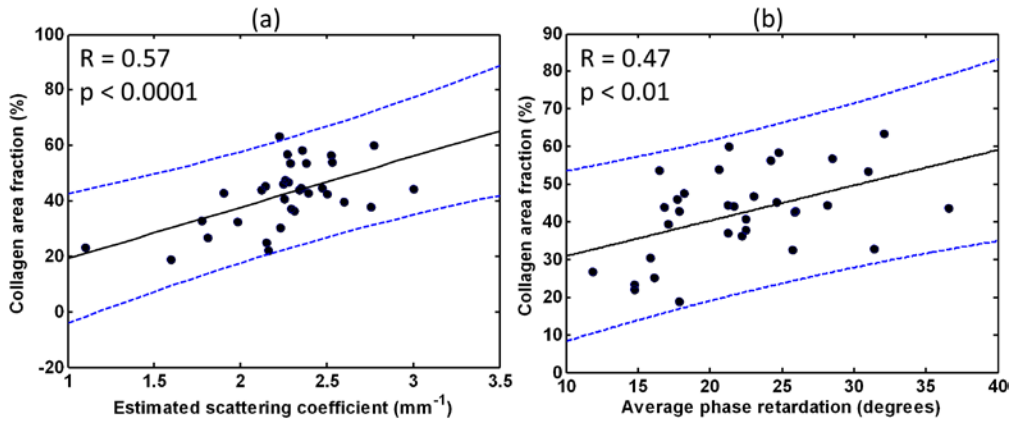

Fig. 7. (a) Positive correlation demonstration between estimated scattering coefficient and collagen content; (b) Positive correlation demonstration between phase retardation and collagen content. The blue dashed lines show 95% prediction intervals.

as exact as OCT images because it is very difficult if not impossible to exactly match the histology slides with OCT cross-section imaging planes.

It is interesting to observe from Fig. 5 (b) and Fig. 6 that the average phase retardation of cancer cases spreads out in a large range and a simple threshold is not adequate to separate the cancers from normal ovaries. However, a good correlation coefficient of R = 0.7 (p = 0.079) was obtained between average phase retardation and average CAF of 7 cancer cases. Because CAF from Sirius Red staining directly evaluates collagen, the positive correlation suggests the phase retardation may measure the complex collagen developmental process of ovarian cancers. Future efforts will be devoted to validating the initial results with a larger patient pool, upgrading the time domain PS-OCT system to a Fourier domain system, and developing a catheter based probe for *in vivo* inspection of ovaries during minimally invasive surgery.

4. Summary

In this report, we studied 33 ovaries obtained from 18 patients using the PSOCT system. Optical scattering coefficient was quantitatively estimated by fitting conventional OCT signal to a single scattering model. A specificity of 100% and a sensitivity of 86% were achieved. Average phase retardation was calculated from PSOCT phase retardation image. A specificity of 100% and a sensitivity of 43% were achieved. Combining estimated scattering coefficient and phase retardation for each ovary, a superior specificity of 100% and a sensitivity of 100% were achieved. Collagen content as assessed by Sirius Red staining correlates strongly with estimated scattering coefficient and phase retardation. These initial results show PSOCT could be a powerful tool to characterize ovarian tissue and to detect ovarian cancers.

Acknowledgments

The authors acknowledge the partial funding support from National Cancer Institute 1R01CA151570 and the Donaghue Foundation.

#164882 - $15.00 USD Received 21 Mar 2012; revised 14 May 2012; accepted 18 May 2012; published 7 Jun 2012